Mayer (NMR spectra) is also acknowledged. We are grateful to J. Y. Huot for valuable advice concerning the preparation of $Ag_2(Suc)_2 \cdot H_2O$ and to J. Lessard for making available a preprint of his paper.

Registry No. $(Suc)_2 \cdot Ag_2 \cdot H_2O$, 91191-42-3; $Ag_2(Suc)_2 \cdot H_2O$ complex, 91191-44-5; $Li[Ag(Suc)_2]$, 91191-41-2; $Na[Ag(Suc)_2]$, 91191-43-4; $Ag_2(Pht)_2$, 41505-30-0; K(Pht), 1074-82-4.

Supplementary Material Available: Infrared wavenumbers of succinimide and the silver complexes (Table IV), ^1H and ^{13}C NMR chemical shifts of phthalimide and some of its derivatives (Table V), geometries of various succinimide compounds (Table VI), details on the $Ag_2(Suc)_2 \cdot H_2O$ crystal structure including refined temperature factors (Table VII), weighted least-squares planes (Table VIII), distances involving the hydrogen atoms (Table IX), and observed and calculated structure factor amplitudes (Table X), details on the $Li[Ag(Suc)_2] \cdot 4H_2O$ structure including refined temperature factors (Table XI), weighted least-squares planes (Table XII), distances involving the hydrogen atoms (Table XIII), and observed and calculated structure factor amplitudes (Table XIV), and infrared spectra of succinimide and its silver complexes (Figure 6) (36 pages). Ordering information is given on any current masthead page.

Contribution from the Molecular Theory Laboratory, The Rockefeller University, Palo Alto, California 94304, and Department of Chemistry, University of Connecticut, Storrs, Connecticut 06268

An INDO Study of [1.1]Ferrocenophane as a Catalyst for Hydrogen Liberation from Aqueous Acidic Media

A. WALEH,*† G. H. LOEW,† and U. T. MUELLER-WESTERHOFF‡

Received May 17, 1983

INDO–SCF calculations with constrained geometry optimization have been carried out to help elucidate the mechanism by which hydrogen gas is liberated when [1.1]ferrocenophane is dissolved in acid media. The calculated equilibrium geometries correspond to protonation at ring carbon atoms. The calculated electronic structures of these species indicate large electron transfer from the rings to the protons. In order to more completely model the protonation and hydrogen liberation processes, single-point energies and electronic structures were obtained for other selected protonated species consisting of various positions of the protons relative to the crystal geometry of the [1.1]ferrocenophane. The results indicate that proton transfers around the rings and between the rings and the metal centers are necessary for these processes. Hydrogen liberation appears to occur by homolytic cleavage of metal–hydrogen bonds from a higher energy conformation, different from the crystal geometry, obtained from twisting of the molecule, leading to the formation of molecular hydrogen and a stable dication.

Introduction

The compound [1.1]ferrocenophene shows several unusual properties due to (a) the proximity of its two ferrocene units, which are linked together by two bridging methylene groups, and (b) the high degree of flexibility of the molecule around these methylene bridges. NMR studies of [1.1]-ferrocenophane[1] show that the molecule undergoes a rapid syn–syn exchange, which, due to a small activation barrier, occurs at a fast rate on the NMR time scale even at low temperatures. Clearly, the exceptional ability of the molecule to undergo rapid conformational change and to accommodate charge relaxations, mediated by the metal centers, is crucial to its function and properties.

An important property of [1.1]ferrocenophane is that the compound dissolves in strong nonoxidizing acids with evolution of hydrogen gas, leaving a stable dication that can be quantitatively reduced to the neutral species.[2] This property, together with the feasibility of large-quantity production of the compound by new synthetic routes,[1,3,4] makes [1.1]-ferrocenophane an attractive candidate as a semiconductor surface modifier[5,6] for use in the photochemical splitting of water in solar energy systems.

Since the oxidation of [1.1]ferrocenophane in aqeuous acids is immediate, no direct observation of the intermediates in the protonation and hydrogen-liberation pathways has been possible. It has been suggested[2] that protonation of [1.1]-ferrocenophane occurs at both iron atoms of the ferrocenyl moieties, consistent with the metal protonation of ferrocenes,[2,7,8] substituted ferrocenes,[8,9] and [*n*]ferrocenophanes.[10] Elimination of H_2 could then follow by a twisting of the molecule into a conformation that would place the hydrogen atoms within bonding distance. However, the exact protonation pathways in ferrocenes and ferrocenophanes and, in particular, the relative importance of the metal and cyclopentadienyl rings in this process have been the subject of much controversy.[11-14] Proton transfer to the ring is evidenced by the "rapid" (>>benzene) deuteration of ferrocene in deuterated acid $BF_3 \cdot D_2O$ and by observed isotopic ratios of 10:3:1 for H_2:HD:D_2 liberation by [1.1]ferrocenophane in deuterated acid.[15]

In view of the importance of the mechanisms of protonation and hydrogen liberation to the function of [1.1]ferrocenophane as a semiconductor surface modifier, and in the absence of direct experimental evidence, characterization of these path-

†The Rockefeller University.
‡University of Connecticut.

(1) Cassen, A.; Eilbracht, P.; Nazzal, A.; Proessdorf, W.; Mueller-Westerhoff, U. T. *J. Am. Chem. Soc.* **1981**, *103*, 6367.
(2) Bitterwolf, T. E.; Ling, A. C. *J. Organomet. Chem.* **1973**, *57*, C15.
(3) Cassens, A.; Eilbracht, P.; Mueller-Westerhoff, U. T.; Nazzal, A.; Neuenschwander, M.; Proessdorf, W. *J. Organomet. Chem.* **1981**, *205*, C17.
(4) Mueller-Westerhoff, U. T.; Nazzal, A.; Proessdorf, W. *J. Organomet. Chem.* **1981**, *205*, C21.
(5) Wrighton, M. S.; Palazzotto, M. C.; Bocarsly, A. B.; Bolts, J. M.; Fischer, A. B.; Nadjo, L. *J. Am. Chem. Soc.* **1978**, *100*, 7264.
(6) Nazzal, A.; Mueller-Westerhoff, U. T., submitted for publication.
(7) Curphey, T. J.; Santer, J. O.; Rosenblum, M.; Richards, J. H. *J. Am. Chem. Soc.* **1960**, *82*, 5249.
(8) Bitterwolf, T. E.; Ling, A. C. *J. Organomet. Chem.* **1972**, *40*, 197.
(9) Bitterwolf, T. E.; Ling, A. C. *J. Organomet. Chem.* **1977**, *141*, 355.
(10) Bitterwolf, T. E.; Ling, A. C. *J. Organomet. Chem.* **1981**, *215*, 77.
(11) Floris, B.; Illuminati, G.; Ortaggi, G. *Tetrahedron Lett.* **1972**, 269.
(12) Floris, B.; Illuminati, G.; Jones, P. E.; Ortaggi, G. *Coord. Chem. Rev.* **1972**, *8*, 39.
(13) Cerichelli, G.; Illuminti, G.; Ortaggi, G.; Giuliani, A. M. *J. Organomet. Chem.* **1977**, *127*, 357.
(14) Bitterwolf, T. E. *Tetrahedron Lett.* **1981**, *22*, 2627.
(15) Bitterwolf, T. E., private communication.

0020-1669/84/1323-2859$01.50/0

ways by theoretical methods and, particularly, elucidation of the charge-transfer process involved in this reduction and the role of the iron and cyclopentadienyl rings are of interest. To this end, we have used a semiempirical INDO–SCF method with transition-metal capability[16,17] to characterize the electron distributions, geometries, and energetics of the species involved in the protonation and hydrogen-liberation processes. We have previously shown[16] that the use of this semiempirical INDO–SCF–CI method with a set of spectroscopic parameters provides a reasonable description of the electronic structure and spectra of ferrocene and ferrocenium ion in agreement with the observed photoelectric and electronic spectra and the results of ab initio calculations. Further, in a complementary part of the present study involving calculations of the ground-state electronic structure of [1.1]ferrocenophane and its carbanion and carbocation derivatives,[18] we have used this same method with appropriate parameters for geometry optimization calculations, under the constrained conditions of fixed ring–ring separation distance, to obtain reasonable geometries for [1.1]ferrocenophane systems. In a continued study of these systems, we report here the results of the calculations of the electronic structure and equilibrium geometries of protonated [1.1]ferrocenophane and other species selected to model the processes of protonation and hydrogen liberation.

Method

A detailed description of the INDO–SCF–CI method has been given previously.[16] Spectroscopic parameterization, in which the two-electron repulsion integrals are evaluated from an empirical Weiss–Mataga–Nishimoto formula,[16,19,20] is ideally suited to the calculation of ground-state electronic structure and properties of transition-metal complexes in their equilibrium geometries. The method also has the capability of performing geometry optimization by a gradient technique in the Cartesian coordinate system with the appropriate parameterization, in which the two-electron repulsion integrals are calculated theoretically and the resonance integrals are set to values suitable for energy calculations. Equilibrium geometries of the protonated [1.1]ferrocenophane were calculated by using the crystal structure of the neutral species[21,22] as the starting geometry and by initially placing two additional hydrogen atoms at various locations inside the molecule and requiring an overall molecular charge of 2+. As we have described in detail elsewhere,[18] the present INDO method, similar to ab initio techniques,[23,24] predicts a cyclopentadienyl ring separation of 3.74 Å larger than the observed value of 3.3 Å.[22] Therefore, all optimization calculations were carried out with the additional constraints of holding the z components of all ring carbon atoms constant in a Cartesian coordinate system in which the y-axis coincides with the axis of C_2 symmetry of the molecule and the iron atoms are positioned on the x axis.

The inclusion of these constraints, which effectively restrict the metal–ligand distance to the experimentally observed value, is important for proper description of the charge distribution and relaxation effects.[18] However, calculations with and

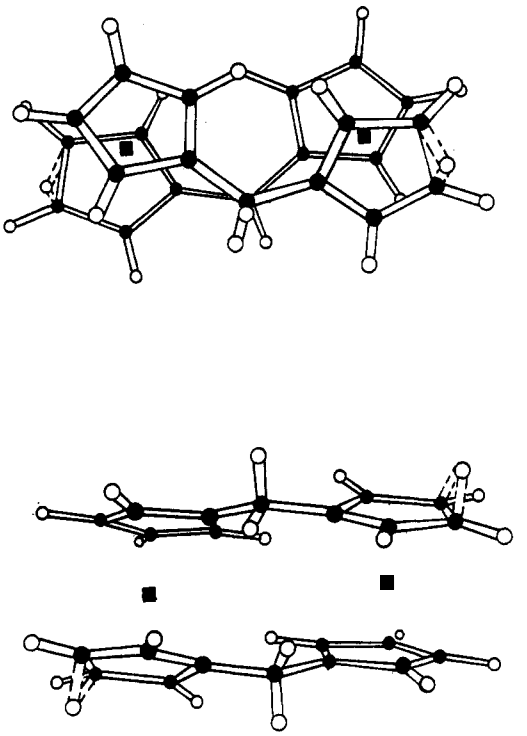

Figure 1. Top and side views of the optimized geometry of β-protonated [1.1]ferrocenophane with two hydrogen atoms initially positioned 1.1 Å from each metal atom on the outside. Symbols: ■, Fe; ●, carbon; ○, hydrogen.

without constraints show that they do not severely affect the details of the equilibrium geometry of the protonated species. In this regard, we note that although seemingly better transition-metal–ligand bond distances have recently been reported for other approximate SCF models,[25] Hartree–Fock and CI investigations of ferrocene and ferrocenium ion indicate that, for a correct description of the metal–ligand distance, electron correlation effects have to be included.[26] Thus, the failure of the INDO–SCF–CI method in correctly describing the metal–ligand distance in ferrocenophane may be a general problem of the Hartree–Fock model in predicting the equilibrium geometry of transition-metal complexes.[24] However, this failure will not severely affect the description of the electronic structure of the ligands themselves, and their proton affinity should be qualitatively correctly predicted. Extensive ab initio studies of the equilibrium geometry of the ferrocene, using from minimal to better than polarized triple-ζ quality basis sets,[23,24] show that in spite of a poor metal–ligand distance, the details of the ligand structure can be properly reproduced at the Hartree–Fock level.

Electronic structures of the protonated species in their equilibrium geometries were obtained by using their optimized geometries as input to the INDO program with spectroscopic parameterization. In addition to the optimized geometries that represent the most stable form of the protonated [1.1]ferrocenophane, single-point calculations of relative energies and electronic structures were also made for two other types of complex geometries. (1) Two hydrogen atoms were placed at varied distances from the iron atoms to investigate the effect of metal protonation. (2) A molecular hydrogen was placed at several locations near the center and at increasing distances from the center of the molecule as a model for the hydrogen formation and liberation. All single-point calculations were

(16) Zerner, M. C.; Loew, G. H.; Kirchner, R. F.; Mueller-Westerhoff, U. T. *J. Am. Chem. Soc.* **1980**, *102*, 589.
(17) Bacon, A. D.; Zerner, M. C. *Theor. Chim. Acta* **1979**, *53*, 21.
(18) Waleh, A.; Cher, M. L.; Loew, G. H.; Mueller-Westerhoff, U. T. *Theor. Chim. Acta*, in press.
(19) Weiss, K., unpublished results.
(20) Mataga, N.; Nishimoto, K. *Z. Phys. Chem. (Wiesbaden)* **1957**, *13*, 140.
(21) McKechnie, J. S.; Bersted, B.; Paul, I. C.; Watts, W. E. *J. Organomet. Chem.* **1967**, *8*, P29.
(22) McKechnie, J. S.; Maier, C. A.; Bersted, B.; Paul, I. C. *J. Chem. Soc., Perkin Trans. 2* **1973**, 138.
(23) Lüthi, H. P.; Ammeter, J.; Almlöf, J.; Korsell, K. *Chem. Phys. Lett.* **1980**, *69*, 540.
(24) Lüthi, H. P.; Ammeter, J. H.; Almlöf, J.; Faegri, Jr. *J. Chem. Phys.* **1982**, *77*, 2002.
(25) Marynick, D. S.; Axe, F. U.; Kirkpatrick, C. M.; Throckmorton, L. *Chem. Phys. Lett.* **1983**, *99*, 406.
(26) Lüthi, H. P., private communication.

Table I. Electronic Properties of Protonated [1.1]Ferrocenophane

	I[a]	II[a]	III[b]	IV[b]	V[b]	VI[b]
			Charges			
Fe	1.781+[c]	1.763+[c]	2.441+	2.278+	2.182+	2.187+
H^+	0.223+	0.210+	0.120−	0.021+	0.021+	0.00+
			d-Orbital Population			
d_{z^2}	1.436	1.431	1.540	1.468	1.031	1.007
$d_{x^2-y^2}$	1.655	1.671	1.481	1.503	1.763	1.764
d_{xy}	1.596	1.564	1.730	1.742	1.754	1.760
d_{xz}	0.847	0.839	0.964	0.961	1.006	1.019
d_{yz}	1.172	1.201	0.991	1.00	0.984	0.986
			HOMO			
energy, au	−0.529	−0.541	−0.561	−0.524	−0.487	−0.436
% character						
d_{z^2}				38.0	69.6	68.8
$d_{x^2-y^2}$	38.3	34.1	65.2	37.3		
d_{xy}	36.8	38.4				
d_{xz}	10.8	13.7		4.6	2.9	4.0
d_{yz}			4.7	2.0	14.8	14.5
C π			13.2			
H^+ s			2.6			
			LUMO			
energy, au	−0.198	−0.211	−0.227	−0.353	−0.383	−0.436[d]
% character						
d_{z^2}			8.4	20.6	67.8	70.3
$d_{x^2-y^2}$	4.9		14.6	20.6		
d_{xy}	4.7	10.6			3.4	3.3
d_{xz}	7.1	5.8		2.0	14.3	14.6
d_{yz}						
C π	57.6	56.2	26.2	22.9		
H^+ s	6.3	6.3	39.0	16.6		

[a] Optimized geometry. [b] Crystal geometry. [c] Metal charges are sensitive to the angle of twist (see text). [d] This orbital is singly occupied and, therefore, is formally a HOMO.

carried out with the crystal geometry of [1.1]ferrocenophane.

Results

One major result of the present calculations is that, under the constrained geometry optimization conditions of fixed ring–ring separation employed, all the equilibrium geometries of protonated [1.1]ferrocenophane obtained correspond to protonation at the ring carbon atoms, independent of the initial position of the protons. Equilibrium complex geometries were calculated with two H atoms initially positioned near the two iron atoms, corresponding to metal protonation, and also within bonding distance of each other (0.74 Å) in the exterior of the molecule. In all cases, optimization causes each of the hydrogen atoms to move to within bonding distance of the nearest ring carbon atoms. Figures 1 and 2 display the top and side views of two optimized equilibrium geometries obtained by initially placing two hydrogen atoms on the x axis at 1.1 Å from each of the iron atoms, outside and inside of the metal centers, respectively. In both cases, the hydrogen atoms move to bind to the nearest ring carbons at the β-position (Figure 1) and α-position (Figure 2), respectively, by displacing the hydrogen atoms initially bonded to those carbons. The protonated ring carbon does not become a tetrahedral sp^3 center. Instead, as shown in Figures 1 and 2, the protonating H atom is shared equally by two neighboring carbon atoms with $r_{C-H} \simeq 1.3$ Å. The distance of this H atom to the other carbon atoms of the same ring are 2.2 and 2.7 Å, respectively.

Ring protonation was also obtained when the H atoms were initially placed, as molecular hydrogen, in the interior of the molecule with the center of the H_2 0.2 Å from the center of the ferrocenophane molecule on the y axis toward the bridge carbons. In the corresponding optimized equilibrium geometry (not shown), the hydrogen atoms moved apart and again protonated their nearest ring carbon atoms, in this case the tertiary carbons. The protonating H atoms in this instance remained in the interior of the molecule with $r_{C-H} = 1.16$ Å and $r_{Fe-H} = 1.96$ Å.

Protonations at various ring positions then correspond to local minima of the potential surface. The most favored configuration corresponds to protonation at the β-carbon atoms (Figure 1) with the protonation at the α-position (Figure 2) about 13 kcal/mol higher in energy. Protonation of the tertiary carbon atoms is at a still higher energy of 124 kcal/mol. No local minima were obtained corresponding to metal protonation.

Geometry optimization calculations for protonated ferrocene, with and without constraints, also show that ring protonation is favored. Furthermore, the ring protonation tendency also remains a dominant feature of the metal-protonated ferrocene obtained by restricting the protonating H atom to the metal plane, in an otherwise constraint-free optimization. Both rings are considerably tilted to establish a C–H distance of 1.42 Å for the nearest carbon atom of each ring, with Fe–H = 1.96 Å. Calculations of charge distributions show that ring protonation of ferrocene is consistent with the large negative charges calculated for the cyclopentadienyl ring carbons. They further indicate that metal protonation requires considerable charge transfer between the metal and ring system and leaves the formal oxidation state of the metal unchanged.

To simulate H_2 liberation, single-point energy calculations with the H_2 molecule at increasing distances from the center of the [1.1]ferrocenophane dication were also made. The total energy was found to decrease with increasing H_2–dication distance, indicating formation of a stable hydrogen molecule once H_2 is moved to the exterior of [1.1]ferrocenophane.

In addition to their energy and optimized geometry, the electronic structure of each of these same representative species in the protonation and H_2-liberation processes was calculated. Table I contains the results of the Mulliken population analysis for atomic charges on the iron atoms and protonating hydrogens, the iron d-orbital populations, and the energies and nature of the highest occupied (HOMO) and lowest unoccupied (LUMO) molecular orbitals for (1) the ring-protonated complexes shown in Figures 1 (case I) and 2 (case II), (2) a

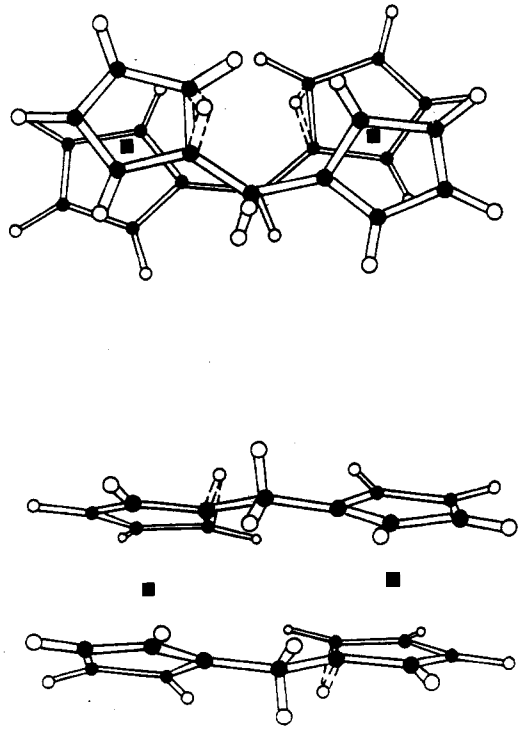

Figure 2. Top and side views of the optimized geometry of α-protonated [1.1]ferrocenophane with two hydrogen atoms initially positioned 1.1 Å from each metal atom on the inside. Symbols: ■, Fe; ●, carbon; ○, hydrogen.

complex where the protons are bound to the Fe atoms with an Fe–H distance of 1.56 Å and an H–H distance of 1.50 Å (case III), and (3) a series of three steps in the liberation of H_2 molecule from the [1.1]ferrocenophane dication with varying distances from the center of each molecule of 0.2 Å (case IV), 3.0 Å (case V), and 10.0 Å (case VI).

The calculated charges show a large net electron transfer to the protons whether they add to the metal (III) or the ring carbon atoms (I, II), resulting in their reduction to atomic hydrogens. The two-electron equivalent charge transfer to the protons, leading to the eventual homolytic cleavage of Fe–H bonds and separation of the molecular hydrogen (IV–VI), is accompanied by only a small change in the charge of the iron atoms. The electron density transferred comes mainly from the cyclopentadienyl anion rings, which substantially decrease in negative charge while the net charges on iron atoms remain close to 2+ throughout the protonation and hydrogen-liberation processes. We should note that the rather large apparent differences between the calculated charges on the irons in I and II compared to those in III–VI in Table I are mainly due to the differences between the optimized and crystal geometries used in the two sets of calculations and not the site of proton bonding. The optimized geometries used in I and II have a larger angle of twist compared to that observed in the crystal geometry.[18,22] The angle of twist is defined as the mean of the angles of projection made by two nearest carbons, one from each ring of the ferrocene unit, viewed down the line joining the center of mass of the two rings.[22] Both the charge distribution between the iron and cyclopentadienyl rings and d-orbital populations are sensitive to the relaxation of this angle.[18] For comparison, the calculated net charge on the iron in neutral [1.1]ferrocenophane is 1.67+ and 2.06+ for optimized and crystal geometries, respectively.

The total electron transfer to the protonating H atoms is sensitive to the Fe–H distance and is greater when the H atoms are within bonding distance of the metal (III). While the net charge on the iron does not increase to 3+ in the dication (VI), the resulting state, similar to the $2A_1'$ state in ferrocenium ion,[16] corresponds to the formal removal of one $3d_{z^2}$ electron from each of the ferrocenes. However, as in the case of the ferrocene and ferrocenium ion,[16] both back-donation into the formally unoccupied d_{xz} and d_{yz} orbitals and forward donation from the formally occupied d_{z^2} orbital result in significant relaxation and reduction of charge buildup on the iron atoms.

Comparison of the nature and energies of HOMO and LUMO in Table I provides further insight into the electronic rearrangements and, particularly, the crucial importance of the metal-protonation step in the course of the hydrogen liberation. While HOMO and LUMO are well separated in energy in the protonated species (I–III), their energy difference is decreased as the hydrogen atoms approach each other and the metal (IV, V) and, finally, they become degenerate and each is singly occupied in the extreme case of dication formation (VI). In particular, the orbital characters show that metal protonation (III) and formation of a hydrogen molecule inside [1.1]ferrocenophane (IV), which involve considerable mixing of the metal d_{z^2} and hydrogen s orbitals, also correspond to the onset and emergence of the dication character, respectively. This illustrates that the electron transfer from metal to hydrogen is formally out of the d_{z^2} orbital. It further shows that the liberation of the H_2 as represented in case V can occur by homolytic cleavage of the Fe–H bond.

Discussion and Conclusions

Under the constrained geometry optimization conditions used, ring protonation was found to be energetically favored over metal protonation of [1.1]ferrocenophane. The NMR spectra of ferrocenes and bridge ferrocenes have been interpreted in terms of metal protonation.[2,7–10] While the constraints used and other approximations inherent in the method do not preclude that protonation at the metal sites could be of comparable or lower energy, possibly due to ring tilting,[8] the results obtained do indicate that proton transfer to cyclopentadienyl rings play an important role in the protonation and hydrogen-liberation processes. A rapid proton exchange around the rings and between the rings and the metal centers, as our results suggest, would also be consistent with the observed NMR spectra of the protonated bridged ferrocenes,[2] if the exchange occurs at very fast rates on the NMR time scale.

The main conclusions of our study can be summarized as follows. (1) Protonations at metal sites and at the ring carbons both lead to large electron donation to the protons from the metal–ring systems, resulting in their reduction to atomic hydrogen character. However, the electron donation is maximized when the hydrogen is bonded to the iron, which indicates that hydrogen transfer to metal is the first step toward molecular hydrogen formation. (2) In the configurations corresponding to crystal geometry, formation of molecular hydrogen inside the [1.1]ferrocenophane is of higher energy than that for both metal- and ring-protonated complexes. Formation of a stable H_2 molecule thus requires an activated configuration of the complex and possibly involves twisting of the molecule. (3) The transition state in the liberation of H_2 corresponds to formation of molecular hydrogen in the vicinity (0.2 Å) of the center of the [1.1]ferrocenophane molecule. At this point there is considerable mixing of the metal d_{z^2} and hydrogen s atomic orbitals, and the energy difference between HOMO and LUMO is decreased. (4) Liberation of molecular hydrogen from this point on is a downhill process in energy, leading to the formation of a stable dication with a pair of singly occupied degenerate d_{z^2} orbitals.

On the basis of these conclusions, the following series of events for the protonation and hydrogen-liberation processes can be suggested. Subsequent to the initial protonation step either at the rings or at the metal centers, the protons are rapidly exchanged between the metals and the rings. In a

particular higher energy conformation, brought about by the twisting of the molecule, in which two hydrogens with a small positive charge, both in the vicinity of the metals, and at near-bonding distances, homolytic cleavage of the hydrogens will occur and molecular hydrogen will be liberated. The rapid proton exchange between the metal and rings and around the ring system, as suggested by the present calculations, is consistent with the observation[15] that when [1.1]ferrocenophane is dissolved in fully deuterated acid $BF_3 \cdot D_2O$, an isotopic mixture of composition 10:3:1 H_2:HD:D_2 is liberated.

Acknowledgment. A.W. and G.H.L. gratefully acknowledge support for this work from NSF Grant PCM7921591.

Registry No. [1.1]Ferrocenophane, 1294-39-9.

Contribution from the Department of Chemistry, Faculty of Science, Hiroshima University, Hiroshima 730, Japan

Structure and Properties of a Cobalt(III) Complex with a Branched Cyclic Tetraamine Ligand, (6-Methyl-6-(4-amino-2-azabutyl)-1,4-diazacycloheptane)(ethylenediamine)cobalt(III) Perchlorate

KANJI TOMIOKA, USHIO SAKAGUCHI, and HAYAMI YONEDA*

Received November 29, 1983

The preparation and properties of a cobalt(III) complex with a new branched cyclic tetraamine ligand, $[Co(L)(en)](ClO_4)_3$, are described, where L is 6-methyl-6-(4-amino-2-azabutyl)-1,4-diazacycloheptane and en is ethylenediamine. The structure of the red complex $[Co(C_9H_{22}N_4)(C_2H_8N_2)](ClO_4)_3$ has been determined by single-crystal X-ray diffraction techniques (R = 0.0462, orthorhombic crystals, space group *Pbca* with a = 14.059 (3) Å, b = 15.319 (5) Å, c = 20.497 (6) Å, and Z = 8). The cobalt(III) ion is surrounded by six nitrogen atoms, four from L and two from en. The N–Co–N angle subtended by the two nitrogens of the 1,4-diazacycloheptane moiety is unusually small (76.4 (1)°). While the Co–N bonds trans to these two nitrogens have normal lengths, the other four Co–N bonds are elongated due to steric strain in the L ligand and the steric repulsion between the hydrogens of L and en. The correlation between the λ_{max} values in absorption spectra and the average Co–N lengths of $[Co(N)_6]$ complexes has been found and used to explain the large red shift in the absorption spectrum of this complex.

Introduction

In a recent series of papers,[1,2] we have been studying the stereoselective association in solution between trigonal $[Co(N)_6]^{3+}$ complexes and *d*-tartrate or bis(μ-*d*-tartrato)diantimonate(III) ion. In that work, we have improved the synthetic method of $[Co(sen)]^{3+}$ for large-scale synthesis, where sen is 1,1,1-tris(4-amino-2-azabutyl)ethane. During the synthesis of $[Co(sen)]^{3+}$, a red crystalline compound was isolated in a yield comparable to that of $[Co(sen)]^{3+}$. The visible absorption spectrum of this compound in water appeared to be consistent with the *cis*-$[Co(O)_2(N)_4]$ chromophore. The chemical analysis was not, however, consistent with any complex involving such a chromophore. The proton NMR spectrum in deuterium oxide was very complex at 60 MHz and was not very helpful in deducing the structure of the compound. Thus, the compound was subjected to the structure determination by single-crystal X-ray diffraction, and it is disclosed that the compound was of the $[Co(N)_6]$ type and contained a novel branched cyclic tetraamine ligand, 6-methyl-6-(4-amino-2-azabutyl)-1,4-diazacycloheptane (L). This paper describes the preparation, spectral characteristics, and structure of the complex, as well as a discussion on the origin of the large red shift in the absorption spectrum of this compound.

Experimental Section

Preparation of $[Co(sen)]^{3+}$ and $[Co(L)(en)]^{3+}$. 1,1,1-Tris(hydroxymethyl)ethane was tosylated in pyridine after Heinz and Burkhardt.[3] The tritosylate (100 g) was refluxed with a large excess of anhydrous ethylenediamine (en) (500 g) for 72 h out of contact with atmospheric moisture and carbon dioxide. Excess en was removed by a rotary evaporator, a solution of sodium hydroxide (240 g) in water (400 mL) was added to the viscous yellow residue, and this mixture then was extracted three times with pyridine (1 L). The extracts were rotary evaporated to give a viscous yellow oil, to which 300 mL of ethanol was added. The mixture was suction filtered to remove *p*-toluenesulfonic acid salts, and this ethanolic solution of crude sen (containing also L and en) was used directly in the subsequent reaction.

Sixty grams of *trans*-$[CoCl_2(py)_4]Cl$[4] (py = pyridine) in 1 L of warm methanol was added, with stirring, to the above ethanolic solution. The orange precipitate of $[Co(sen)]Cl_3$ that was formed was suction filtered, washed with ethanol and ether, and recrystallized from warm water, yielding 35 g of analytically pure $[Co(sen)]Cl_3$. The overall yield based on the starting material 1,1,1-tris(hydroxymethyl)ethane was about 60%. To the dark red-brown filtrate was added a further amount (30 g) of *trans*-$[CoCl_2(py)_4]Cl$ with mechanical stirring, and the solution was concentrated by a rotary evaporator, yielding a red precipitate. This was the chloride salt of $[Co(L)(en)]^{3+}$, which was collected by filtration. Because the chloride salt was rather hygroscopic, it was transformed into the perchlorate salt by using an anion-exchange column of QAE-Sephadex A-25 (perchlorate form). The effluent was concentrated on a rotary evaporator, and the precipitate was collected by filtration. The perchlorate salt was recrystallized from warm water, and its yield was about 20 g (19% based on the tritosylate). Anal. Calcd for $[Co(C_{11}H_{30}N_6)](ClO_4)_3$: C, 21.89; H, 5.01; N, 13.92. Found: C, 21.90; H, 5.31; N, 14.00.

Measurements. Proton magnetic resonance spectra were obtained on a JEOL JNM PMX-60 spectrometer at 60 MHz and 37 °C, with an internal standard of sodium 4,4-dimethyl-4-sila-1-pentanesulfonate (DSS). Electronic absorption spectra were obtained on a Shimadzu UV-240 double-beam recording spectrophotometer at ambient temperature.

The optical resolution of $[Co(L)(en)]^{3+}$ was effected by reversed-phase ion-pair chromatography with 0.01 M potassium bis(μ-*d*-tartrato)diantimonate(III) as the ion-pairing reagent.[5] The column packing was LS-410 ODS.SIL. (Toyo Soda Manufacturing

(1) Sakaguchi, U.; Tsuge, A.; Yoneda, H. *Inorg. Chem.* **1983**, *22*, 1630.
(2) Sakaguchi, U.; Tsuge, A.; Yoneda, H. *Inorg. Chem.* **1983**, *22*, 3745.
(3) Heinz, F.; Burkhardt, R. *Chem. Ber.* **1957**, *90*, 921.
(4) Werner, A.; Feenstra, R. *Chem. Ber.* **1906**, *39*, 1538.
(5) Izumoto, S.; Sakaguchi, U.; Yoneda, H. *Bull. Chem. Soc. Jpn.* **1983**, *56*, 1646.

0020-1669/84/1323-2863$01.50/0